Timing and style of Late Quaternary glaciation in the eastern Hindu Kush, Chitral, northern Pakistan: a review and revision of the glacial chronology based on new optically stimulated luminescence dating

Lewis A. Owen[a,*], Ulrich Kamp[b], Joel Q. Spencer[a,1], Klaus Haserodt[c]

[a] *Department of Earth Sciences, University of California, Riverside, CA 92521-0423, USA*
[b] *Department of Geography and Geology, University of Nebraska at Omaha, Omaha, NE 68182-0199, USA*
[c] *Department of Environment and Society, Institute of Geography, Technical University Berlin, Rohrdamm 20-22, 13629 Berlin, Germany*

Abstract

Glacial landforms and sediments provide evidence for two Late Quaternary major glaciations in the eastern Hindu Kush. New optically stimulated luminescence (OSL) dating was undertaken to define the timing of these glaciations and associated sediment deposition. The Drosh Glacial, was defined by OSL dating to have occurred during marine isotopic stage-3, producing an extensive valley glaciation that extended to an altitude of $\geqslant 1300$ m above sea level (asl) in the main valley, with an equilibrium line altitude (ELA) depression of ~ 1200 m. The Pret Glacial produced a valley glaciation that extended to an altitude of ~ 1670 m asl. in the main valley, with an ELA depression of ~ 1000 m. The new OSL dating suggests that this glacial stage probably represents several glacial advances that occurred during the latter part of the Last Glacial. Moraines representing two minor glacial advances, the Shandur and Barum Glacial stages, were also recognized near the contemporary glaciers. These probably formed during the Middle/Late Holocene and Little Ice Age, respectively. This study and comparisons with adjacent regions suggest that there was limited glaciation during the global Last Glacial Maximum (LGM) in the Hindu Kush. Deglaciation in the mountain ranges of the Himalayas and the consequent meltwater discharge into the adjacent seas was negligible immediately after the global LGM and it was therefore of minor importance as a forcing factor for global climate change during the end of the last glacial cycle. However, our studies show that glaciation and particularly deglaciation is important in controlling the deposition of thick valley fills and the landscape evolution of the high mountain environments. © 2002 Elsevier Science Ltd and INQUA. All rights reserved.

1. Introduction

The mountains of the Himalaya, including the Hindu Kush and Karakoram Mountains, have the largest concentration of glaciers outside of the Polar Regions. These are drained by some of the world's greatest rivers including the Indus and Ganges–Brahmaputra systems. The south Asian summer monsoon and the mid-latitude westerlies supply precipitation to these mountains to feed the glaciers and rivers. Variations in the south Asian summer monsoon and the mid-latitude westerlies control the nature and extent of glaciation in this region. This in turn affects the hydrology of the glaciers and river systems. Meltwaters from these glacial systems supply substantial quantities of freshwater into the adjacent Arabian Sea and Bay of Bengal and probably are important in influencing ocean circulation and, in turn, influence regional and global climate. Changes in glaciation and hydrology throughout the Late Quaternary are poorly understood despite the possibility that large quantities of meltwater could have drained into the adjacent seas during deglaciation. Substantial inputs of freshwater may have a major impact on ocean circulation and global climate similar to the effects of the melting of the Laurentide ice sheet in the North Atlantic Ocean (cf. Broecker et al., 1989). Despite this little is known of the extent and timing of former and recent glaciation throughout the mountains of the Himalaya and Tibet.

In this paper, we present new evidence for the timing and extent of Late Quaternary glaciation in the eastern Hindu Kush Mountains. This region is situated at the western most end of the Hindu Kush–Karakoram mountain belt in northern Pakistan (Fig. 1). This paper

---

*Corresponding author. Tel.: +1-909-787-3106; fax: +1-909-787-4324.

E-mail address: lewis.owen@ucr.edu (L.A. Owen).

[1] Present address: School of Geography and Geosciences, University of St Andrews, St Andrews, Fife, KY16 9AL, Scotland.

reviews, refines and presents a new interpretation of the glacial history of this region that was originally presented in Kamp's (1999) doctoral thesis and partially summarized in Kamp (2001a, b). Our fresh interpretation of this Late Quaternary history is based on new optically stimulated luminescence (OSL) dating that was undertaken after Kamp (1999, 2001a, b). In this paper, we are now able to test whether former glaciation in the Hindu Kush, Karakoram and West-Himalaya was synchronous with fluctuations in the south Asian summer monsoon or with the Northern Hemisphere ice sheets and oceans. Quaternary valley fills and landforms in the Chitral and adjacent valleys of the eastern Hindu Kush are described to develop relative chronologies and to undertake OSL dating. This will help to define the extent and timing of glaciation and to aid in the elucidation of the evolution of high mountain landscapes. Furthermore, the Hindu Kush is particularly important in helping assess the potential significance of glaciation and freshwater input into the Arabian Sea. The extent and timing of Quaternary glaciation is important for assessing changing surface and boundary conditions for paleoclimatic modeling.

2. Regional setting

The research area is situated in the Chitral District of northern Pakistan and covers an area of $\sim 14,500\,\text{km}^2$ (Fig. 1). Geologically the region comprises a complex assemblage of rocks of different ages. The topography is a consequence of the collision of the Indian and Eurasian continental plates that was initiated ~ 50 million years ago. The Hindu Kush is still actively deforming, and together with the Pamirs, they constitute the most seismically active intermediate-depth seismic zone in the world. Much of the Hindu Kush comprises metamorphosed sedimentary rocks of amphibolite and greenschist facies, metamorphosed granodiorite, and tourmaline rich leucogranites. Structurally, the Hindu Kush is bounded to the south by a right lateral strike-slip fault, the Heart fault, but the northern margin is less

Fig. 1. Location map of the main study area in Chitral, northern Pakistan.

well defined. The main suites of rocks, faults and mountain ranges trend NNE into the Hindu Raj (Searle, 1991). The Chitral River is the main drainage originating at an altitude of 3000 m asl and flows SW for a distance of 300 km to join the Kunar and Kabul Rivers in Afghanistan, which eventually flow into the Indus River and on into the Arabian Sea. The Hindu Kush mountains have altitudes of between 5500 and 7500 m asl with the highest peak, Tirich Mir, rising to 7706 m asl, while in the SE part of the study area the Hindu Raj rise to altitudes of between 5000 and 7000 m asl. Approximately 34% of the study area lies above 4500 m asl with a snowline rising northwards across the study area from ~4800 to ~5000 m asl (Haserodt, 1995). The region experiences a subtropical-Mediterranean climate influenced by the mid-latitude westerlies and the Southwest Asian summer monsoon. The mean monthly temperature at Chitral Town rises from 4°C (January) to 28°C (July). The precipitation decreases from SW to NE (e.g. mean annual rainfall at Drosh is more than 600 mm, while at Chitral Town it is ~450 mm); but in the high glacier region precipitation may be four times as much. Occasional summer heavy rainfall occurs, partly influenced by the superposition of a marginal monsoon influence in the south and influences of western disturbances at high altitudes. There is considerable annual rainfall variability from year to year (Haserodt, 1995). Vegetation type varies with altitude from steppe of *Artemisia* at elevations up to ~3200–3600 m asl, alpine scrub and meadows up to ~3800–4100 m asl and subnival pioneer vegetation at the highest elevations.

3. Field methods

Landforms were mapped along the Chitral and Mastuj valleys in the Hindu Kush at a scale of 1:250,000 (U502 Series), 1:126,720 and 1:63,360 (Survey of India from 1929–1933), and at 1:10,000 for selected areas after Kneisel et al. (1998). Furthermore, different composites of a Landsat-5 TM satellite image (151-35) from 23 August 1995 helped to identify geomorphic forms. Established procedures using field survey techniques and a global positioning system to establish location, aided by barometric altimetry, were used following the methods of Derbyshire and Owen (1990) and Owen et al. (1995). These maps are presented in Kamp (1999). The morphology of the landforms was described and where possible sedimentary sections were examined within each landform using the standard sedimentary logging techniques of Tucker (1982) and Eyles et al. (1983). Using the criteria of Owen (1994), care was taken to distinguish glacial and non-glacial diamicts because of the widespread mass movement and rapid resedimentation of deposits in this

region. Relative chronologies were established using standard morphostratigraphic techniques (Rose and Menzies, 1996).

Sites were chosen for the collection of samples for OSL dating on the basis of the relative chronologies. A variety of lithologies were chosen for each formation and glacial stage to provide a range of particle sizes and depositional environments to maximize the potential of dating the deposits. The OSL samples were obtained by hammering opaque plastic tubes into cleaned sections. Once removed the tubes were sealed in plastic and placed in light-tight sampling bags. Sub-samples were collected to provide material to cross check OSL sample moisture content and for neutron activation analysis (NAA). All the samples remained sealed until opened in the laboratory. Table 1 and Fig. 5 provide details of the sample locations and geomorphic settings.

4. Relative chronologies

Fig. 2 schematically illustrates the relative ages of the main landforms and formations in the Chitral and the adjacent valleys. Detailed descriptions of these are provided in Kamp (1999, 2001a, b), but their important and salient details, starting with the oldest landforms and deposits, are reproduced below to provide a review and setting for understanding the glacial geology and the revised chronology and interpretation.

4.1. Drosh Glacial stage

Evidence for this glaciation comprises ice scoured bedrock and scattered till patches along the floors of a series of palaeovalleys that are perched ~80–150 m above the contemporary river and along the valley sides south of Chitral Town (Fig. 3; Fig. 4a) and within the Mastuj valley (Fig. 5H). Subglacial meltwater erosional features like glacier mills are also present along the valley sides (Fig. 4b). Evidence for an extensive valley glacier can be traced along the Lower Chitral valley as far south as Drosh at an altitude of 1300 m asl. Ice-contact glaciolacustrine and glaciofluvial sediments relating to this stage are also present along the valley sides throughout the main Chitral valley (Figs. 5A, B, E, F and H, and Fig. 6).

4.2. Broz Formation

The Broz Formation comprises fanglomerates up to 350 m thick that form large fans that extend into the axis of the valley (Fig. 7). The fans are highly dissected and comprise meter-bedded stratified matrix-supported bouldery diamicts (Fig. 5C and D).

Table 1
Summary of OSL dating results from 90–125 μm quartz extracted from sediment matrices: sample locations, radionuclide concentrations, moisture contents, total dose-rates, D_e estimates and optical ages

Sample no.	Location (N, E)	asl (m)	Depth (cm)	U[a] (ppm)	Th[a] (ppm)	K[a] (%)	Rb[a] (ppm)	$W_{in\ situ}$[b] (%)	Cosmic[c] (mGya^{-1})	Dose-rate[d] (mGya^{-1})	n[e]	Mean D_e[f] (Gy)	Age (ka)
C47	35°46.93′, 71°46.72′	1580	300	2.34	9.18	1.79	91.1	2.6	0.186	3.09±0.20	5	126.50±7.01	40.9±3.5
C48	35°43.17′, 71°46.99′	1520	500	2.84	11.7	1.59	106	1.3	0.147	3.18±0.20	9	129.16±8.54	40.6±3.7
C51	35°42.96′, 71°45.16′	1580	400	3.32	18.9	2.6	125	3.1	0.166	4.72±0.30	9	109.24±8.25	17.5–27.8[g]
C52	35°42.96′, 71°45.16′	1580	520	2.98	15.3	2.45	124	4.5	0.146	4.17±0.27	4	130.79±8.72	31.4±2.9
C53	35°43.14′, 71°45.65′	1500	2700	2.57	12.6	2.29	117	1.3	0.029	3.77±0.26	10	80.86±5.19	21.5±2.0
C55	35°45.64′, 71°47.08′	1480	250	1.48	8.29	1.36	85.4	1.5	0.193	2.46±0.16	7	123.54±8.34	50.3±4.7
C56	35°35.83′, 71°49.01′	1475	450	3.43	14.7	1.91	119	5.9	0.154	3.68±0.23	3	134.55±7.04	36.6±3.0
C61	36°16.56′, 72°28.51′	2150	400	4.71	15.3	1.96	117	1.0	0.183	4.31±0.27	3	33.36±2.84	7.7±0.8
C62	36°16.36′, 72°22.14′	2230	300	2.66	18.1	3.29	147	4.1	0.208	5.13±0.35	9	190.28±18.45	27.0–55.2[g]

[a] Elemental concentrations from NAA of whole sediment measured at Becquerel Laboratories, Lucas Heights, NSW, Australia. Uncertainty taken as ±10%.

[b] Estimated fractional water content from whole sediment (Aitken, 1998). Uncertainty taken as ±5%.

[c] Estimated contribution to dose-rate from cosmic rays calculated according to Prescott and Hutton (1994). Uncertainty taken as ±10%.

[d] Total dose-rate from beta, gamma and cosmic components. Beta attenuation factors for U, Th and K compositions calculated using Rainer Grün's "Age" program incorporating grain size factors from Mejdahl (1979). Beta attenuation factor for Rb arbitrarily taken as 0.75 (cf. Adamiec and Aitken, 1998). Factors utilized to convert elemental concentrations to beta and gamma dose-rates from Adamiec and Aitken (1998) and beta and gamma components attenuated for moisture content.

[e] Number of replicated D_e estimates used to calculate mean D_e—also indicated in Table 2. The maximum number of replicated measurements was limited by hardware constraints. The low value of n for C52, C56 and C61 is due to poor quartz yields.

[f] Mean equivalent dose (D_e) determined from replicated single-aliquot regenerative-dose (SAR; Murray and Wintle, 2000) runs. Errors are 1-sigma standard errors (i.e. $\sigma_{n-1}/n^{1/2}$) incorporating error from beta source estimated at about ±5%.

[g] The wide scatter in D_e results for C51 and C62 (see Table 2) suggest acute heterogeneous partial bleaching. The OSL ages are bracketed between the minimum and maximum D_e results corresponding to an age range of about 17.5–27.8 ka for C51 and 27.0–55.2 ka for C62, respectively.
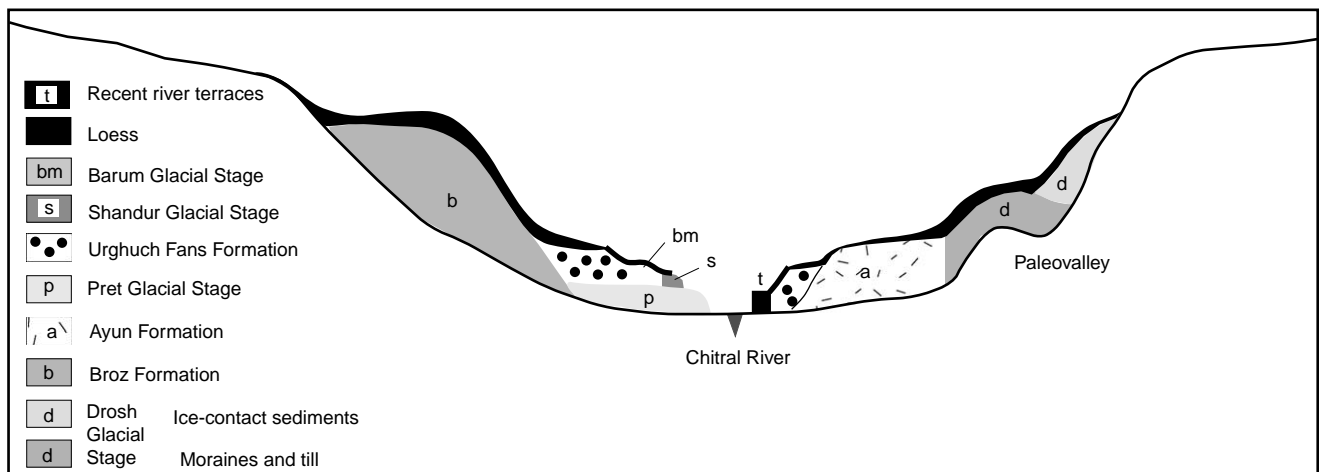
Fig. 2. Schematic section across the Chitral valley showing the main landforms and sediments, and their relative ages. The relative positions of each OSL dating sample are shown in relation to the main landforms and sediments.

4.3. Ayun Formation

The Ayun Formation is an extensive valley fill exceeding 170 m in thickness, comprising rounded polymictic pebbles and cobbles (Fig. 7, labeled a). It locally overlies the Drosh Glacial Stage sediments and the Broz Formation.

4.4. Pret Glacial Stage

This comprises a well-preserved succession of moraines within the main Mastuj and Yarkhun valley and their tributaries (Fig. 8). Moraines of this stage can be traced along the Mastuj valley to Pret at an altitude of ∼1670 m asl. Drumlinised moraines are present on a
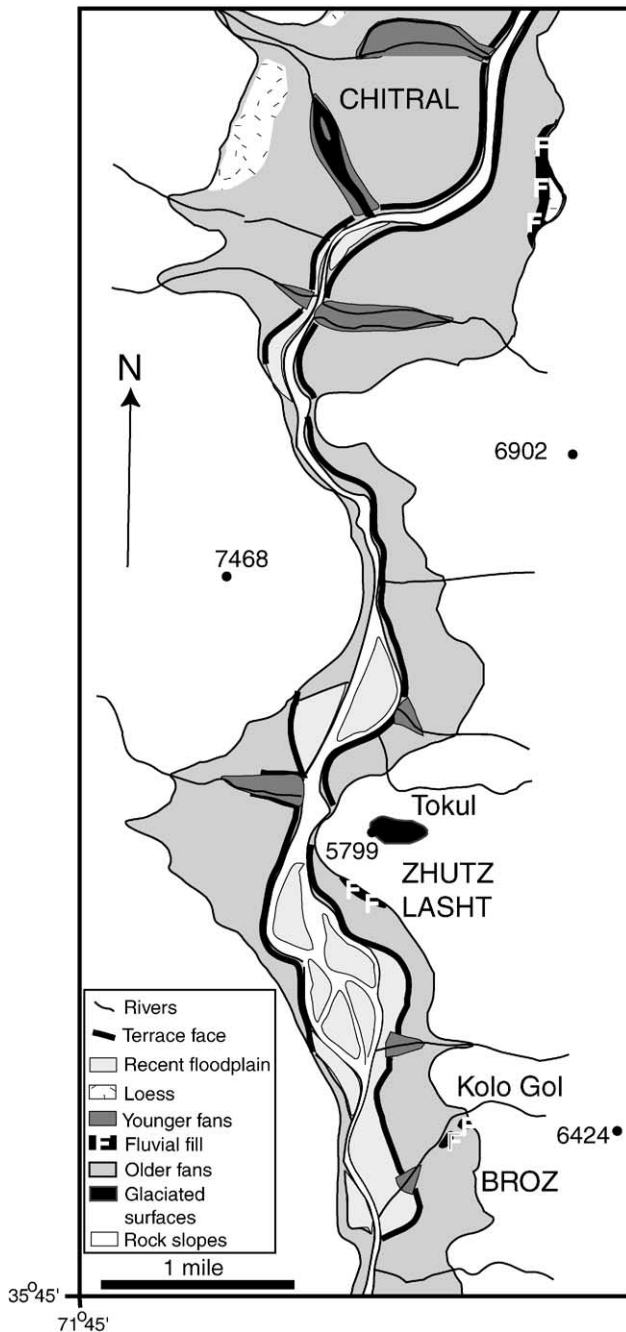
Fig. 3. Geomorphic map showing the main landforms in the Chitral valley south of Chitral Town in Lower Chitral.

bedrock plateau between Mastuj and Turkho rivers. Glaciotectonized sediments of this stage are also present along the valley floor to the west of Mastuj (Fig. 5G).

4.5. Sonoghar Glacial Sub-Stage

A set of very distinctive sharp-crested end and lateral moraines are present near the mouths of some of the tributary valleys in upper Chitral. These are assigned to

the Sonoghar Sub-Stage within the Pret Glacial. Particularly good examples of these can be found in the Mastuj valley at Sonoghar, in the Lutkho valley at Garam Chashma, and in the Laspur valley.

4.6. Urghuch Formation

The Urghuch Formation is composed of meter-bedded debris flow and fluvial units that form a distinct set of fans. These sediments and landforms are closely associated with eroded landforms of the Broz Formation, the Ayun Formation and moraines of the Pret and Sonoghar Glacial Stages. The fans are complex, exhibiting several phases of incision and progradation (Figs. 4 and 7 labeled u). Many of these fans are still active and at some locations they are prograding into the center of the valley.

4.7. Loess

Loess mantles most of the landforms throughout the Chitral valley and much of the Mastuj valley. The loess reaches a thickness of up to 10 m in the Chitral and Mastuj valley. The loess commonly contains pebbles and boulders representing considerable colluvial input.

4.8. Shandur Glacial Stage

Two sets of well-formed moraines are present on the western side of the Shandur Pass that has an altitude of ~3700 m asl. These are assigned to Shandur I and II Glacial Stages. The moraines of the outer, older moraines (Shandur I) slope ~13° and are ~20 m high, while the inner, younger moraines (Shandur II) slope ~20–30° and are ~40 m high.

4.9. Barum Glacial Stage

Two sets of sharp crested moraines are present within a few hundred meters of the contemporary glaciers and these are assigned to the Barum I and II Glacial Stages. In the Barum valley, the lateral moraines of the Barum-I Glacial Stage are 100 m high and are actively eroding on their proximal sides. These moraines reach down to ~3200 m asl. In many places the moraines are covered with granitic boulders up to several meters in diameter. The moraines are less weathered than the Shandur moraines. A distinct younger set of moraines, the Barum-II Glacial Stage, is inset into the Barum-I Stage.

4.10. Recent river terraces and floodplains

The contemporary river is complex, consisting of many braids and meanders. Suites of river terraces rise several meters above the present floodplain.
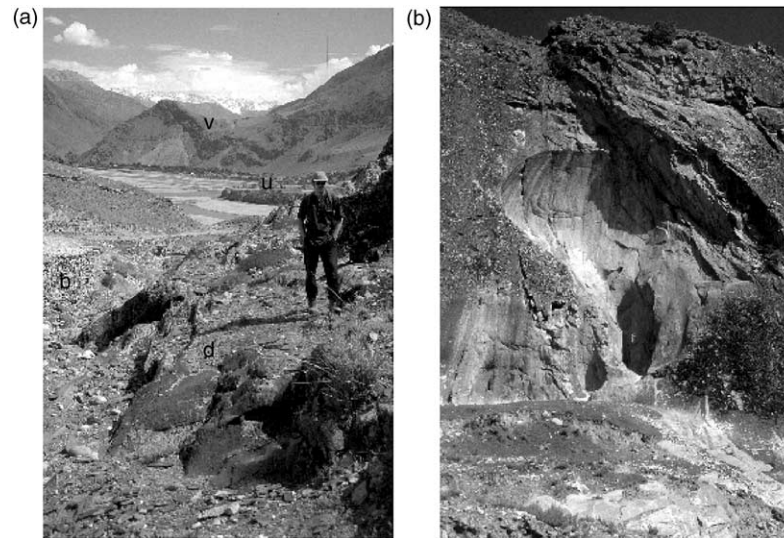
Fig. 4. Landforms of the Drosh Glacial Stage. (a) View looking south across the Chitral valley from near the top of Tokul (35°46.85′N/071°46.89′E at 2610 m asl). A pre-Drosh Glacial Stage paleovalley (labeled v), the Drosh Glacial Stage glacial scoured bedrock (d), fluvial pebbles of the Broz Formation (b) and fans of the Urghuch Formation (u) can be seen in the view. (b) Subglacial erosion cavity on the valley wall between Broz and Ayun (35°40.96′N/071°46.084′E, ∼1400 m asl)

5. Optically stimulated luminescence dating

The preliminary OSL dates presented in Kamp (1999, 2001a, b) and the new OSL dates presented in this study were conducted at the luminescence dating laboratories at the University of California, Riverside. The pre-liminary OSL data presented in Kamp (1999, 2001a, b) were from pilot studies utilizing the infrared stimulated luminescence (IRSL) signal from coarse-grained (90–125 μm) K-rich feldspar fractions (Table 3). Equivalent dose (D_e) estimates from the IRSL measurements were derived using the single aliquot additive dose

Fig. 5. Sampling sites for optically stimulated luminescence dating showing the detailed sedimentology. The numbers shown in each section refer to the descriptions of the sedimentary units. (A) 35°46.934′N/071°46.717′E, 1580 m asl: View looking north at glaciofluvial gravels of the Drosh Glacial Stage that overlie striated bedrock above Zhuti Lasht village. Unit 1—matrix-supported polymictic well rounded pebbles with occasional cobbles and boulders. These are slightly imbricated and are >1.5 m thick; Unit 2—crudely stratified poorly sorted sandy silts with abundant mm-size pebbles; Unit 3—poorly sorted pebbly sands and fine sand layers; Unit 4—very low angled cross-stratified course sands and pebbly sands with mm-size pebbles. (B) 35°43.165′N/071°46.993′E, 1520 m asl: View looking southwards at ice-contact glaciolacustrine sediments of Drosh Glacial Stage in a road cutting on the edge of a deep nala opposite Ayun village. Unit 1—matrix-supported bouldery diamict with crude meter-thick stratification that dips sub-parallel to the slope of the fan. This unit stretches upslope and is at least 18 m thick; Unit 2—cross-stratified medium to fine-grained sands; Unit 3—Planar bedded sands and silts. The lower half of this unit comprises cm-thick beds, dominantly silt. The upper half of the unit has dm-thick beds dominantly sand; Unit 4—trough cross-stratified fine sands and silts comprising channel fills that are between 2–4 m wide and 60—80 cm deep; Unit 5—dm-thick planar beds of sand and silt. (C) 35°42.960′N/071°45.157′E, 1580 m asl: View looking east at a road cutting showing fluvial sediments of the Broz Formation at the northern end of the Ayuns paleovalley. Unit 1—clast-supported well-rounded and sub-spherical cobbles and boulders; Unit 2—planar laminated mm- to cm-thick beds of pebbly medium to fine sands. (D) 35°43.143′N/071°45.646′E, 1500 m asl: view of section along an irrigation dyke along the edge of a large fan of the Broz Formation north of Ayun Nala. Unit 1—well rounded polymictic boulders and cobbles in a pebbly sand matrix. Granites dominate this unit; Unit 2—angular cobble-size slates, with occasional well rounded granite pebbles and cobbles; Unit 3—high angled cross-stratified cm-size pebbles; Unit 4—low-angled planar cross-stratified cm-thick beds of pebbly sands. (E) 35°45.642′N/071°47.075′E, 1480 m asl: View of valley fill deposit near Kolo valley. Unit 1—well rounded imbricated polymictic cobbles and pebbles of glaciofluvial outwash of the Drosh Glacial Stage. These are crudely cross-stratified with dm-thick beds picked out by particle size variations; Unit 2—finely cross-stratified poorly sorted pebbly sands comprising channel fills; Unit 3—cross-stratified cobbles and pebbles. (F) 35°35.826′N/ 071°49.013′E, 1475 m asl: view of lacustrine sediments in a jeep cutting at Lawi that are probably ice-marginal sediments of the Drosh Glacial Stage. Unit 1—pebbly silt with crude stratification subparallel to the surface of the slope; Unit 2—massive matrix-supported bouldery diamict; Unit 3—planar meter-thick bed of laminated silts. (G) 36°16.558′N/072°28.510′E, 2150 m asl: view looking south at a glaciotectonized section of Pret Glacial Stage near river-level west of Mastuj. The sample that was dated (C61) pre-dates the deformation and places a maximum age on the Pret glaciation. Unit 1—massive matrix-supported silty boulder diamict; Unit 2—stratified boulders and cobbles; Unit 3—deformed stratified gravels; Unit 4—deformed planar bedded silts containing small isolated and clusters of dropstones; Unit 5—low-angled cross-stratified cm-size pebbles. (H) 36°16.355′N/072°22.136′E, 2230 m asl: view looking down main valley at a road cutting through a moraine complex of the Drosh Glacial Stage at ∼5 km west of Sonoghur. Unit 1—massive matrix-supported cobble and boulder diamict; Unit 2—sandy silt lens with contorted stratification which stretches for at least 10 m; Unit 3—massive gravelly silt; Unit 4—massive matrix-supported cobbly bouldery diamict.
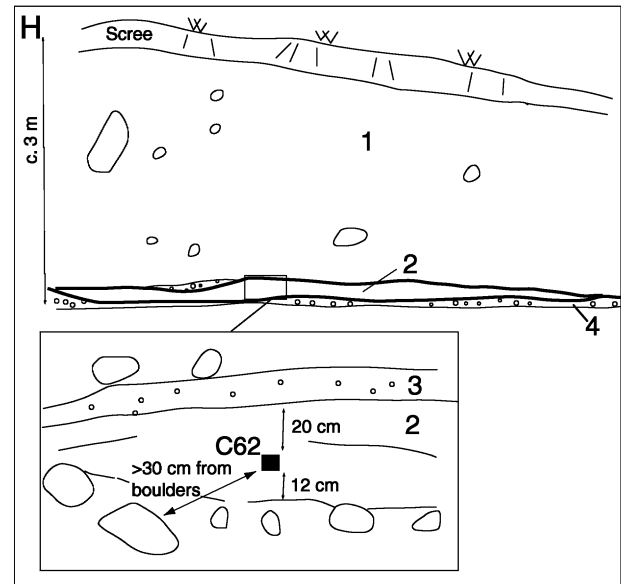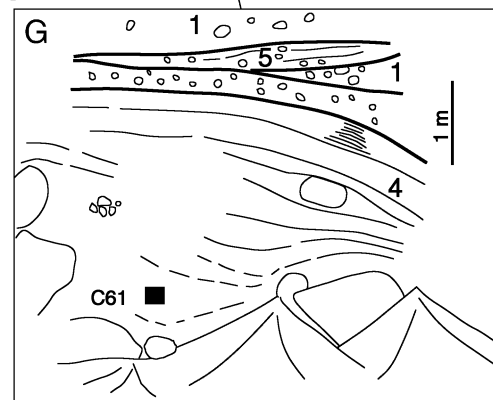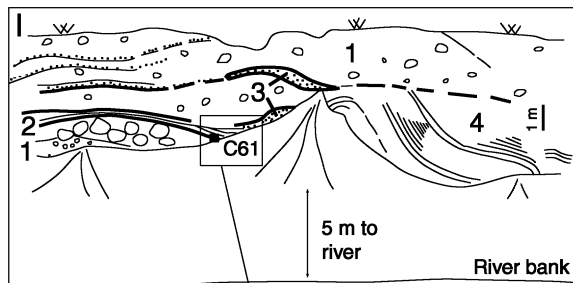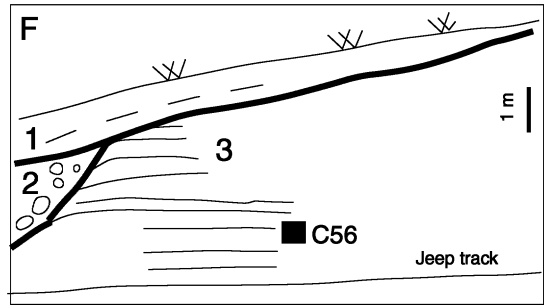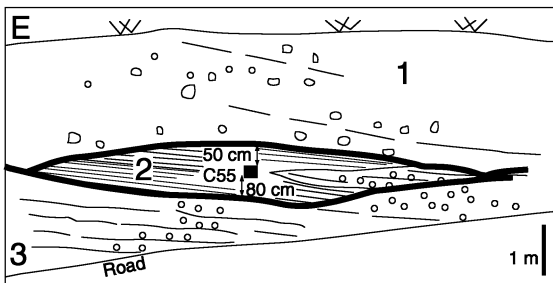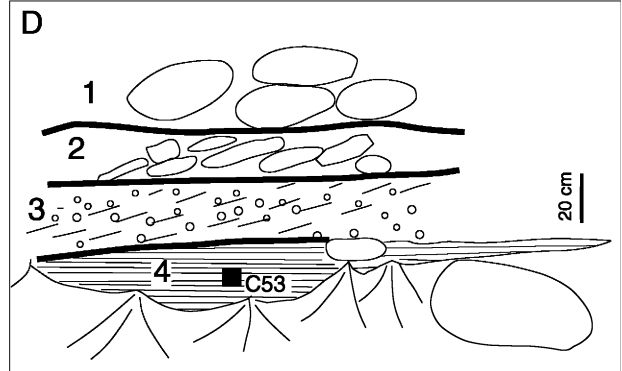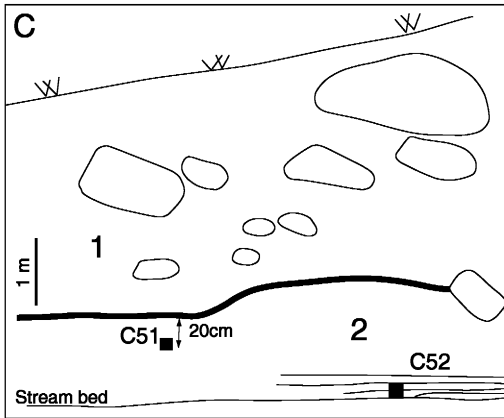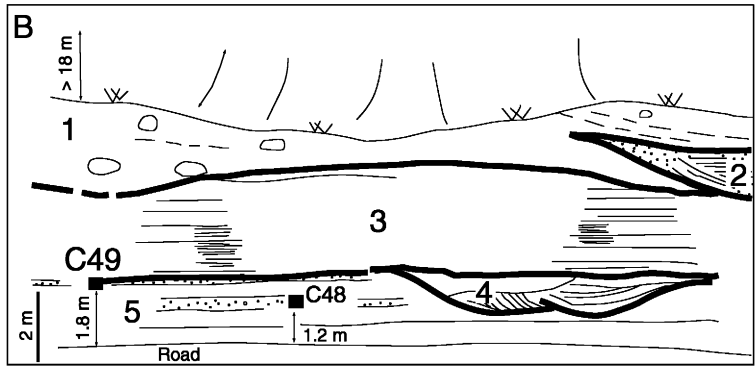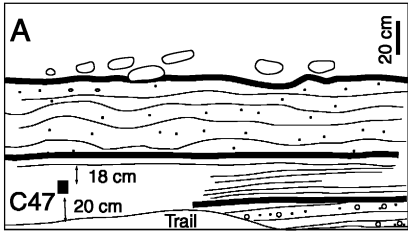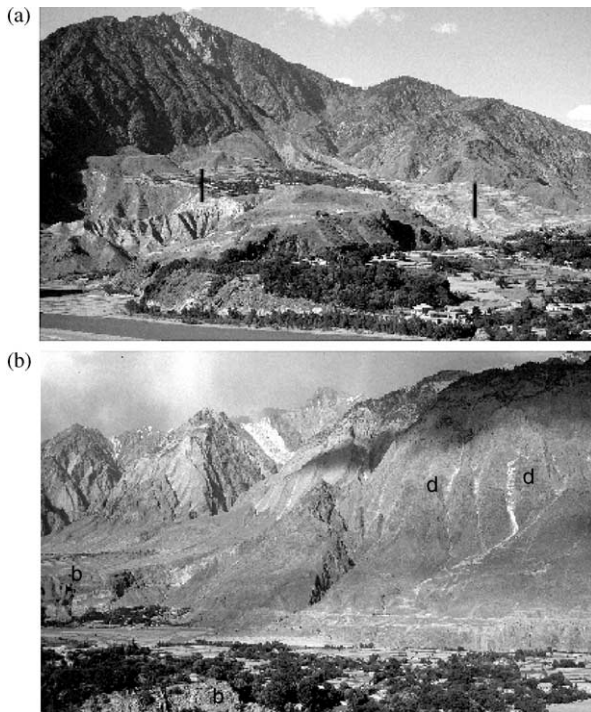
Fig. 6. Glacial landforms and sediments of the Drosh Glacial Stage. (a) Glaciolacustrine sediments (l) at Lawi. (b) Remnants of moraines (d) along the valley sides and the Broz Fan Formation (b) near Mastuj town.

Fig. 7. View looking northward towards Kolo valley from Ayun. Glacial scoured bedrock of Drosh Glacial Stage is present in the foreground (d), the Broz Formation is seen in the distance (b) capped by loess (l), while the Ayun Formation (a) and the Urghuch Formation (u) is present in the middle ground.

Fig. 8. (a) View from Awi at moraines of a deglaciation or readvance stand of the Pret Glacial Stage. (b) View looking south at the moraine ridges (p) opposite Buni (from 36°16.97′N/072°15.56′E, 2140 m asl). A high paleovalley probably of Drosh Glacial Stage is seen in the distance (d). Buni, built on the Urghuch Formation (u), is present to the left of the plate.

(SAAD) technique developed by Duller (1991, 1994). Only one aliquot (additional aliquot for preheat correction) was measured from each sample and a simple linear function was used to extrapolate the corrected additive dose data. Due to evidence of poorer solar bleaching efficiency of remnant luminescence from feldspars (summarized by Aitken, 1998) and the

potential problems with respect to fading and accurate assessment of microdosimetry, we decided to focus the main optical dating of these sediments on the green stimulated luminescence (GSL) or blue–green stimulated luminescence (BGSL) from quartz fractions. Furthermore, the advantages of robust sensitivity correction, recuperation assessment, rapidity of measurement and increased precision via interpolation, made the use of the latest single aliquot regenerative-dose (SAR) protocols developed by Murray and Wintle (2000) an additional attractive prospect.

The preparation of samples in our new study involved estimating in situ water content (mass of moisture/dry mass; Aitken, 1998) from the sub-samples by drying them in an oven at 50°C. The samples for dating were dry sieved to obtain a 90–125 μm particle size fraction. The carbonates and organic matter were removed from the 90–125 μm fraction using 10% HCl and 30% H_2O_2, respectively. Sodium polytungstate solutions of different densities and a centrifuge were used to separate the quartz and feldspar-rich fractions from the heavy minerals. The separated quartz-rich fraction was treated with 49% HF for 30 min to dissolve any plagioclase

feldspars and remove the alpha-irradiated surface of the quartz grains. Several samples (C48, C55, C56 and C62) were treated with H_2SiF_6 acid for 7 days to reduce the infrared-stimulated signal (see below) from contaminant feldspar to a negligible level. Two of these samples (C48 and C62) required an additional 49% HF treatment for 30 min. Dried quartz grains were mounted on stainless steel discs with silicon spray. All the preparation techniques were carried out under laboratory safelights to avoid sample bleaching.

About 20 g of the dried sub-sample from each sediment sample was ground to a fine powder and sent to the Becquerel Laboratories at Lucas Heights in Australia for Neutron Activation Analysis (NAA). Using appropriate dose-rate conversion factors (Adamiec and Aitken, 1998) and beta attenuation factors (see Table 1, note d) the elemental concentrations were converted into external beta and gamma components, which were in turn attenuated for moisture content. These were summed together with a cosmic ray component (estimated using Prescott and Hutton, 1994) to give estimates of the total dose-rate for each sample.

Luminescence measurements were undertaken using a Daybreak 1100 automated system with an 1100FO/L combined fiber-optic/IRLED illuminator for optical stimulation (Bortolot, 1997). Luminescence from the quartz grains was stimulated using a 150 W halogen lamp producing either a broadband blue–green light ($\sim$425–600 nm; $\sim$72 mW cm^{-2}) using the basic excitation filter stack or a green light (514Δ34 nm; $\sim$20 mW cm^{-2}) defined by an additional narrow band interference filter. All quartz samples were screened for feldspar contamination using infrared stimulation from T-1 GaAlAs diodes (880Δ80 nm; diode current 20 mA). All OSL signals were detected with a photomultiplier tube characterized by 9 mm Schott UG11 ultraviolet detection filters. Daybreak TLApplic 4.26 software was used for hardware control and D_e analysis.

D_e measurements were determined using the SAR protocol developed by Murray and Wintle (2000). In the SAR method, each natural or regenerated OSL signal is corrected for changes in sensitivity using the OSL response to a subsequent test dose. The natural dose (N) was measured in the first cycle, and thereafter five regeneration doses (R_1 to R_5) were administered. The first three were used to bracket the natural luminescence level ($R_1 < N \sim R_2 < R_3$), the fourth (R_4) was set at zero to monitor recuperation (i.e. R_4/N) and the fifth dose was made equal to the first to monitor reproducibility (i.e. R_5/R_1) of sensitivity corrections. Each measurement cycle comprised a regeneration dose (zero for natural), a preheat of 200°C for 10 s, optical stimulation for 100 s (sample temperature of 125°C), a constant test-dose, a test-preheat cut after a linear temperature ramp to 160°C and a final optical stimulation for 100 s (at 125°C). The net-natural and net-regenerated OSL were derived by taking the initial OSL signal (0–1 s) and subtracting a background from the last part of the stimulation curve (90–100 s). The net test-dose response was derived by subtracting the background from the preceding natural and regenerative OSL signals.

Multiple D_e estimates were carried out on each sample. The number of replicated measurements was limited both by hardware constraints and poor quartz yields (see Tables 1 and 2). Growth curves were plotted using the net natural and regenerated data divided by the subsequent response to the net-test dose. The growth curve data was fitted with either a single saturating exponential or linear function. Two rejection criteria were utilized; if recuperation was > 5% of the natural level and if the recycling ratio between repeat regenerative levels was > 10%. If a disc failed to meet these criteria the result was discarded and a new disc measured. The distribution in D_e results was analyzed using histogram plots, and in certain cases individual D_e results, which were distinct from a main narrow distribution, were discarded (Table 2). In these instances, the adjusted mean D_e and smaller error were used to calculate final ages. The results for C51 and C62 suggest significant heterogeneous partial bleaching, and therefore, we have used the minimum and maximum D_e values obtained to indicate a possible age range for these samples. Comparisons of these new data with the preliminary results from Kamp (1999) are shown in Table 3. It is clear, even after careful re-evaluation of the data from the original pilot study, that all the ages, apart possibly from sample C62, are very discordant and every feldspar age is higher than the corresponding quartz age.

Even though the feldspar samples were all given linear-additive dose steps between $\sim$100 and $\sim$200 Gy, up to a maximum of $\sim$500 and $\sim$1000 Gy, respectively, the growth in luminescence before correction is poor in all cases. The highest of the additive values, measured after the final additive dose had been administered, is only $\sim$85% of the natural level (C48) and two of the samples effectively exhibited zero growth in luminescence (C51 $\sim$6%; C56 $\sim$−7%). This is a possible indication of large remnant geological luminescence signals, indicating inadequate solar bleaching of the feldspar minerals before deposition. Furthermore, as discussed in Table 3 note b, the SAAD D_e estimates for samples C51, C55 and C56 are likely to be *underestimated*, indicating that the true ages would have an even greater discordance compared with the quartz-SAR results. Other possible reasons that the feldspar ages are overestimated include uncorrected changes in luminescence sensitivity, poor assessment of luminescence background values, and extrapolation uncertainties. For the above reasons we favor the new dating analysis.

Table 2
Equivalent dose (D_e) values from replicated SAR measurements on 90–125 μm quartz extracts

Aliquot #	Equivalent dose values for each single aliquot measured (Gy)[a]								
	C47	C48	C51	C52	C53	C55	C56	C61	C62
1	130.74±8.69	151.34±5.69	100.90±13.11	143.46±19.81	68.64±3.09	98.53±6.96	130.43±12.90	37.57±2.42	238.08±12.01
2	127.48±3.95	142.44±43.81	87.73±5.58	119.60±4.30	71.80±5.56	**156.03±5.45**	136.73±38.97	32.84±5.01	283.24±11.62
3	114.74±3.44	143.91±5.18	128.53±7.71	122.51±13.78	85.29±5.79	129.75±6.40	136.50±8.18	29.67±6.82	138.64±6.17
4	**194.72±16.17**	120.38±4.14	129.79±11.12	137.58±27.66	74.84±5.06	132.59±5.48			154.28±7.70
5	**80.52±6.23**	108.56±4.16	130.98±11.92	**58.69±12.98**	72.11±5.48	132.97±4.00			197.99±7.14
6	128.39±7.18	133.25±6.05	114.12±7.77	**12.27±1.38**	102.51±11.01	120.63±4.75			151.01±6.31
7	131.18±8.62	122.53±3.69	82.69±5.13		84.68±6.17	140.45±4.43			160.58±10.67
8		102.19±5.35	113.40±8.46		82.27±5.64	109.83±3.54			177.39±7.32
9		137.86±7.47	95.04±5.91		90.18±8.29				211.28±10.37
10			170.86±18.76		76.28±4.17				
Results using all D_e data									
Mean D_e	129.68	129.16	115.40	99.02	80.86	127.60	134.55	33.36	190.28
σ_{n-1}	33.86	16.78	26.17	52.13	10.31	17.89	3.57	3.97	47.41
Results with data in bold omitted[b]									
Mean D_e	126.50	129.16	109.24	130.79	80.86	123.54	134.55	33.36	190.28
σ_{n-1}	6.76	16.78	18.53	11.55	10.31	14.82	3.57	3.97	47.41

[a] The maximum number of replicated measurements was limited by hardware constraints. The low number of replicates for C52, C56 and C61 is due to poor quartz yields.

[b] Data was omitted based on two rejection criteria: (a) if the recycling ratio for individual replicated SAR points exceeded 10% or if the mean recycling ratio exceeded 10%; (b) if individual D_e values were significantly remote from the main distribution identified using a histogram plot.

Table 3
Preliminary SAAD K-feldspar IRSL ages after Kamp (1999), re-evaluation of the IRSL data, and comparison with new SAR quartz GSL and BGSL ages

Sample no.	SAAD K-feldspar IRSL ages after Kamp (1999)[a] (ka)	Re-evaluation of SAAD K-feldspar IRSL ages[b]			SAR quartz GSL and BGSL ages[c] (ka)
		D_e (Gy)	Dose-rate (mGya^{-1})	Age (ka)	
C47	149±11	248.0±9.8	3.54±0.25	70.0±6.7	40.9±3.5
C48	130±10	242.0±24.0	3.65±0.26	66.3±8.7	40.6±3.7
C51	78±33	356.8±17.1*	5.18±0.34	68.9±6.6	17.5–27.8
C52	Poor data	Poor data	4.63±0.31	Poor data	31.4±2.9
C53	121±9	234.1±25.5	4.22±0.30	55.5±7.8	21.5±2.0
C55	187±30	432.0±25.3*	2.90±0.22	149.1±16.2	52.0±4.6
C56	75±28	521.0±22.3*	4.13±0.28	126.1±11.8	36.6±3.0
C61	101±10	166.3±43.9	4.77±0.31	34.9±9.7	7.7±0.8
C62	53±5	198.2±30.3	5.62±0.38	35.3±6.2	27.0–55.2

[a] Results from initial pilot study using one aliquot (additional aliquot for preheat correction) per sample. A simple linear function was used to extrapolate the additive data.

[b] This work; re-evaluation of results from Kamp (1999). To re-evaluate the D_e values a small adjustment was made to the additive doses to reflect the most recent beta source calibrations and single saturating exponential functions were fitted to the data. Data was analyzed using the dose correction method described by Duller (1994) except for those values marked with an asterisk (*) where the growth in luminescence was poor and the iterative procedure did not converge. For these samples the luminescence correction (Duller, 1991) was applied, although according to Duller (1994) values > 80 Gy which are non-linear are likely to be underestimated. Slight adjustments were made to the dose-rates by introducing beta attenuation factors based on variations in radionuclide composition (see Table 1, note d). Microdosimetric contribution was assessed by assuming internal K of 10±5% and internal Rb of 0.035±0.015%.

[c] This work; for details see Tables 1 and 2.

6. Discussion

The Hindu Kush landscape reflects a history of uplift, erosion, glaciation and valley sedimentation that produced deep valleys, high peaks and thick valley fills comprising glacial, glaciofluvial, lacustrine, aeolian and mass movement sediments. Using an example from the Chitral valley below Chitral town, Fig. 9 illustrates the typical sequence of landscape forming events that occurred throughout the Hindu Kush during the Late Quaternary. In this example, the main Chitral and Mastuj valleys developed prior to the Drosh Glaciation.
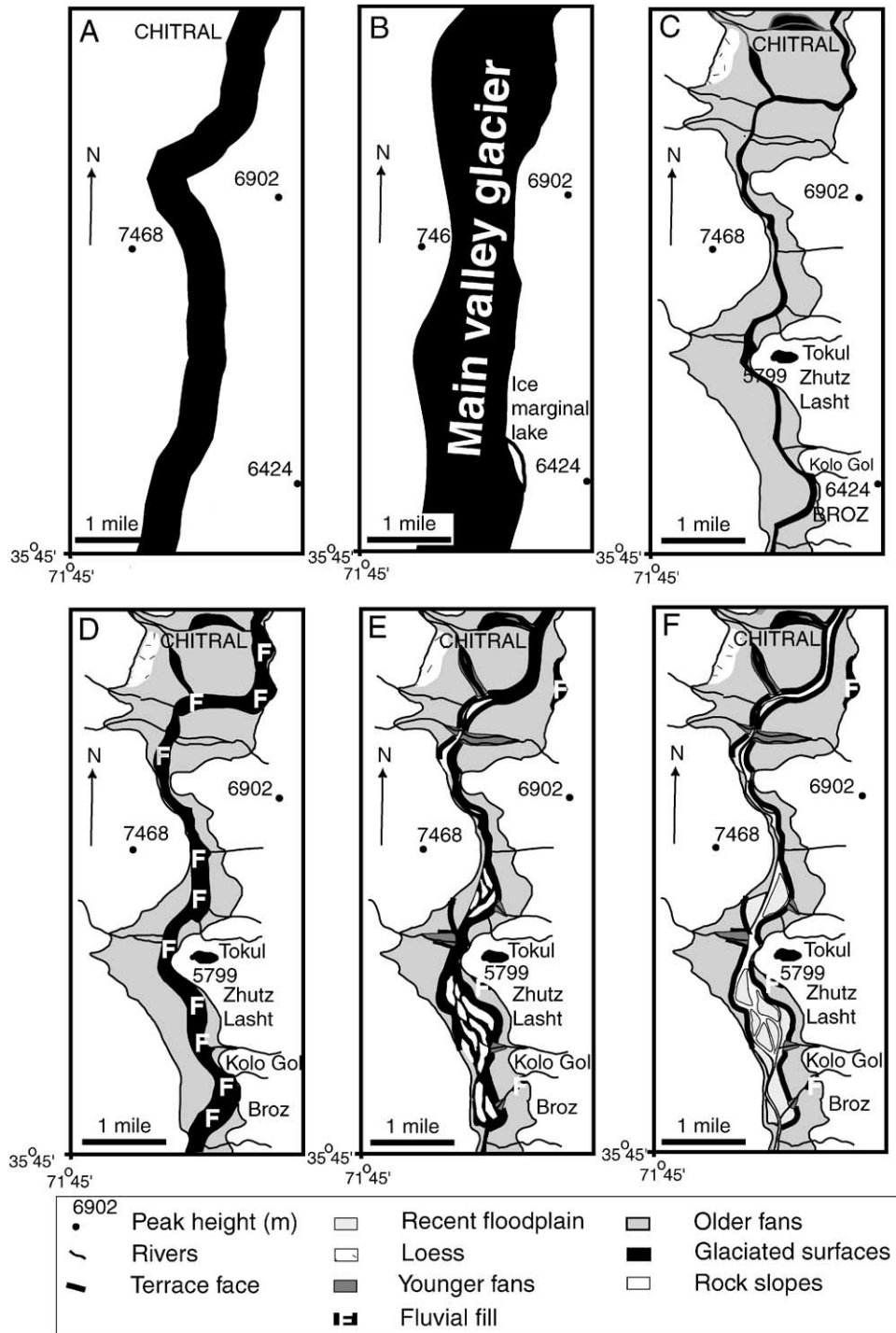
Fig. 9. Sequential development of the upper Chitral Valley. (A) Paleovalley developed during the early Quaternary. (B) Glaciation during the Drosh Glacial Stage (~MIS-3). (C) Formation of paraglacial fans (Broz Formation) shortly after the Drosh Glacial Stage. Loess deposition begins. (D) Incision of the paraglacial fans and deposition of the Ayun Formation by the Chitral River. (E) Incision of the Ayun Formation by the Chitral River and aggradation of fans to form the Urghuch Formation. (F) Fluvial incision to the present day.

Evidence for this is preserved as eroded paleovalleys at elevations of between 80–150 m above the present river level. The Drosh Glacial Stage produced an extensive valley glacier system that extended down the Chitral main valley to an elevation of at least 1300 m asl eroding the paleovalleys and leaving till remnants along the walls of the main Chitral valley and within the paleovalleys. The main valley glacier was at least 500 m thick, 270 km long and based on the methods of Kamp (1999) it had an equilibrium line altitude (ELA)

of 3850 m (an ELA depression of 1200 m compared with contemporary ELAs). On the basis of the new OSL dates (C47, C48, C55, C56 and C62), the Drosh Glacial occurred during marine isotopic stage-3 (MIS-3). However, the precision of the dating technique does not allow us to assign the glaciation to a particular part of MIS-3. These new dates contrast with the former dates presented in Kamp (1999, 2001a, b) that places this glaciation in the penultimate glacial cycle and for the reasons stated in the previous section we favor the new dating analysis.

During deglaciation much of the Drosh Glacial Stage glacial sediment was resedimented to form thick paraglacial fans that filled the Chitral valley and its tributaries to comprise the Broz Formation (Fig. 10). The new OSL dates (C51, C52 and C53) on sediment within one of these fans define its age to the latter part of MIS-3 and/or MIS-2. These dates also contrast with the former dates reported in Kamp (1999, 2001a, b) that place the Broz Formation in the penultimate glacial cycle. However, we believe the new dating analysis and stratigraphy strongly favor our new interpretation of these landforms as being younger than that proposed in Kamp (1999, 2001a, b). The Chitral River and its tributaries subsequently eroded the fans of the Broz Formation. Fluvial sediments of the Ayun Formation were deposited on top of the eroded fans and along axis of valleys. The Ayun Formation was not dated, but it probably represents a period of deposition during MIS-2 and/or the Early Holocene when the climate would have been warmer and wetter, and the fluvial system would have been more dominant than during the proceeding glacial times. Later fluvial processes subsequently eroded the Ayun Formation.

The Pret Glacial Stage probably represents a glacial advance during the latter part of the Last Glacial to Early Holocene. During this glaciation, glaciers advanced down the Mastuj main valley and its tributaries to Pret at an altitude of 1670 m asl (Fig. 10). The main trunk glacier was ~500 m thick and 200 km long and based on the methods of Kamp (1999) it had an ELA of 4050 m (an ELA depression of ~1000 m compared with contemporary ELAs). In the Sonoghar Stage, tributary glaciers that often reached down into the Mastuj main valley left large end moraines at the mouths of the tributary valleys. This stage may represent a readvance or a still stand toward the end of the Pret Glacial. Only one OSL date was determined for the Pret Glacial (C61) and therefore it is relatively poorly defined, but suggests that ice was still present during the early Holocene. The new OSL date is substantially younger than the date presented in Kamp (1999, 2001a, b) and thus our new chronology shows that the Pret glaciation was younger than previously thought.

The Urghuch Formation began to form as paraglacial fans developed due to the resedimentation of moraines
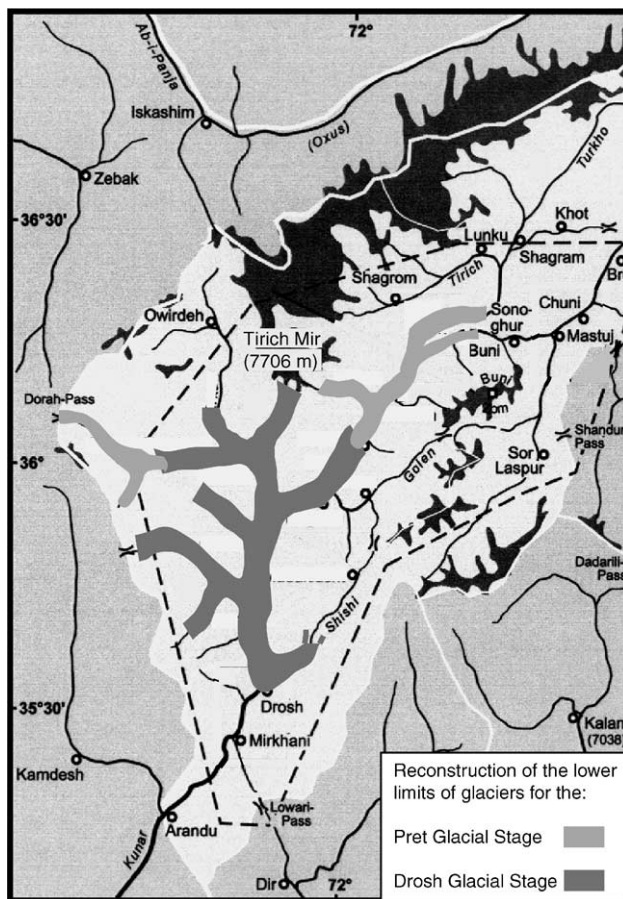
Fig. 10. Reconstruction of the lower limits of glaciation during the Pret and Drosh Glacial Stages.

and older fans during the deglaciation of the Pret and Sonoghar Glacial Stages. The fans that comprise the Urghuch Formation are still active and exhibit varying degrees of aggradation and incision, producing a complex series of terraces and fans.

The Shandur and Barum Glacial Stages followed this period of valley sedimentation. These glacial stages have not been dated, but, comparison with the studies of Haserodt (1989) and Meiners (1995) in northern Pakistan, and the freshness of the large lateral moraines, it is likely that they represent middle/late Holocene and Little Ice Age advances, respectively.

The extensive and moderately thick (~10 m) deposits of loess throughout the region suggest that the loess began to form when the main Chitral and Mastuj valley became ice-free after the Drosh Glacial.

This study, therefore, provides a framework for the temporal and spatial control on the timing of Late Quaternary glaciation and landscape development in Chitral. The most extensive valley glaciation in the Hindu Kush, the Drosh Glacial Stage, occurred early in the last glacial cycle during MIS-3. The stratigraphy, defined by the new OSL dates, compares favorably with

glacial chronologies in adjacent regions of northern Pakistan. These show that the most extensive valley glaciation, the "local" last glacial maximum (LGM), occurred early in the last glacial cycle, probably during MIS-3 (Phillips et al., 2000; Richards et al., 2000a; Owen et al., 2002). These data, therefore, indicate that glaciation in these areas was asynchronous with the Northern Hemisphere ice sheets that reached their maximum extent during the "global" LGM in MIS-2. In addition, there is abundant evidence for several glacial advances during the last glacial cycle and the Holocene (Richards et al., 2000a; Owen et al., 2002). Furthermore, glaciation during the global LGM was limited in many areas of the Himalaya (Phillips et al., 2000; Richards et al., 2000a, b; Owen et al., 2002). Assigning the Pret Glacial Stage to the latter part of the Last Glacial and the Sonoghar Glacial Stage to the Late Glacial/Early Holocene also compares favorably with the glacier advances that have been recognized in other parts of northern Pakistan and the Khumbu Himal (Phillips et al., 2000; Richards et al., 2000a, b; Owen et al., 2002). MIS-3 and the Early Holocene were insolation maxima and during these times the south Asian summer monsoon would have extended further north into the Himalaya to supply increased precipitation as snow at high altitudes. This in turn would have lead to positive glacier mass balances and would have allowed glaciers to advance. Furthermore, Shi Yafeng et al. (1999, 2001) showed using a variety of proxy data that during MIS-3 the summer monsoon over the Tibetan Plateau produced between 40% and over 100% more precipitation than today. Precipitation in Chitral would have increased in a similar manner. Hence, we argue that precipitation changes related to fluctuations in the south Asia summer monsoon, rather than temperature changes, are the major control on the timing and style of glaciation in this part of the Himalayan mountain belt.

The importance of increased snowfall and consequent glacial advances during insolation maximum when the south Asian monsoon is strengthened has important implications for the understanding and modeling of the supply of meltwaters to the oceans. Our data and comparisons with the adjacent regions suggests that glaciers advance during the warmer times of a glacier cycle, while during the coldest times glaciation is restricted because of reduced monsoon precipitation. Furthermore, we have evidence to show that an extensive valley glacier system existed in the Hindu Kush during the latter part of the last glacial cycle and the Early Holocene. This suggests that there would have been little increase in meltwater input into the Indian Ocean via the Indus River system at this time. Thus, it is unlikely that Himalayan glaciers were very important in causing changes in oceanic circulation that may have helped drive Late Quaternary climate change.

Our study also illustrates the close association between glaciation and valley development; in particular the importance of paraglacial processes in modifying Himalayan landscapes. Owen et al. (1995) and Owen and Sharma (1998) suggested similar controls on valley development in other parts of the Himalaya. They were unable, however, to adequately define the ages of the landforms by numerical dating. Our study, therefore, provides a geochronological control on the history of the landscape evolution of a typical Himalayan landscape. Such studies are important for illustrating how retreating glaciers may effect sedimentation and landscape evolution in mountain environments. This is particularly relevant to our understanding of glaciated mountain landscapes that are under threat due to human-induced global warming.

7. Conclusions

This paper provides a review and revision of the evidence for Late Quaternary glaciation of the eastern Hindu Kush. We recognize two major Late Pleistocene glaciations. The oldest glaciation, the Drosh Glacial Stage, occurred during MIS-3 to produce an extensive valley glaciation that extended to an altitude of ≥1,300 m asl in the main valley, and with an ELA depression of ~1200 m. This glaciation was followed during the latter part of MIS-3 and/or MIS-2 by a phase of rapid fan development that was probably the result of resedimentation during the deglaciation of the Drosh Glacial Stage. The younger major glaciation, the Pret Glacial Stage, was more restricted in extent, but extended to an altitude of ~1670 m asl in the main valley with an ELA depression of ~1000 m. This glaciation probably represents several glacial advances that includes the Sonoghar Glacial Sub-Stage. Two minor glacial advances, the Shandur and Barum Glacial Stages, are also recognized near the contemporary glaciers. These were not dated but they probably occurred during the Middle/Late Holocene and/or Little Ice Age, respectively. It is likely that these glaciations in the eastern Hindu Kush are contemporaneous with glaciations in the Hunza and middle Indus valleys.

This study helps support the view that glaciation throughout the mountain ranges of the Himalaya was restricted during the global LGM, and those glacial advances are controlled dominantly by the south Asian summer monsoon. During insolation maximum the south Asian summer monsoon provides increased precipitation as snowfall at high altitudes to cause positive glacier mass balances to allow glaciers to advance. The glaciers advanced during the insolation maximum of MIS-3 and the Late Glacial-Early Holocene. Consequently, meltwater discharge from the Himalayan glaciers via the Indus River system into the

Indian Ocean was not significant enough to influence oceanic circulation and help drive climate change at the end of the last glacial cycle.

The landforms and thick valley fills in the eastern Hindu Kush that comprise fluvial, glaciofluvial, mass movement, glacial and lacustrine sediments are largely controlled by climatic changes that force glacial cycles. In particular, paraglacial processes are important in producing extensive and thick fans that form an important component of these fills. It is apparent that much of the sedimentation that occurs within the valleys in this region occurred as glaciers retreated during paraglacial times. This region provides a good model for how other Himalayan and high mountain landscapes have evolved during Late Quaternary times.

Our study also provides a framework for more detailed geochronological work and we emphasis the need to date the younger moraine successions more precisely to define the nature of glaciation during the end of the last glacial cycle.

References

Adamiec, G., Aitken, M., 1998. Dose-rate conversion factors: update. Ancient TL 16, 37–50.

Aitken, M.J., 1998. An Introduction to Optical Dating. Oxford University Press, Oxford.

Bortolot, V.J., 1997. Improved OSL excitation with fiberoptics and focused lamps. Radiation Measurements 27, 101–106.

Broecker, W.S., Kennett, J.P., Flower, B.P., Teller, J.T., Trumbore, S., Bonani, G., Wolfli, W., 1989. Routing of meltwater from the Laurentide Ice Sheet during the Younger Dryas cold episode. Nature 341, 318–320.

Derbyshire, E., Owen, L.A., 1990. Quaternary alluvial fans in the Karakoram Mountains. In: Rachocki, A.H., Church, M. (Eds.), Alluvial Fans: A field Approach. Wiley, Chichester, pp. 27–53.

Duller, G.A.T., 1991. Equivalent dose determination using single aliquots. Nuclear Tracks Radiation Measurements 18, 371–378.

Duller, G.A.T., 1994. Luminescence dating of sediments using single aliquots: new procedures. Quaternary Geochronology (Quaternary Science Reviews) 13, 149–156.

Eyles, N., Eyles, C.H., Miall, A.D., 1983. Lithofacies types and vertical profile models: an alternative approach to the description and environmental interpretation of glacial diamicts and diamictite sequences. Sedimentology 30, 393–410.

Haserodt, K., 1989. Zur pleistozänen und postglazialen Vergletscherung zwischen Hindukusch, Karakorum und Westhimalaya. In: Haserodt, K. (Ed.), Hochgebirgsräume Nordpakistans im Hindukusch, Karakorum und Westhimalaya. Beiträge und Materialien zur Regionalen Geographie 2, 181–233.

Haserodt, K., 1995. The geographical features and problems of Chitral: a short introduction. International Hindu Kush Conference, Chitral Town, Pakistan, 19 September.

Kamp, U., 1999. Jungquartäre Geomorphologie und Vergletscherung im östlichen Hindukusch, Chitral, Nordpakistan. Berliner Geographische Studien 50, 254.

Kamp, U., 2001a. Jungquartäre Terrassen und Talentwicklung in Chitral, östlicher Hindukusch Zeitschrift für Geomorphologie, 45, 453–475.

Kamp, U., 2001b. Die jungquartäre Vergletscherung Chitrals im östlichen Hindukusch, Pakistan Zeitschrift für Gletscherkunde und Glazialgeologie, 37, 81–100.

Kneisel, C., Lehmkuhl, F., Winkler, S., Tressel, E., Schröder, H., 1998. Legende für geomorphologische Kartierungen in Hochgebirgen (GMK hochgebirge). Trierer Geographische Studien 18, 1–24.

Meiners, S., 1995. Exemplary observations concerning historical to neoglacial glacier stades in the catchmant area of the NW-Karakoram (Hispar Muztagh, Batura Muztagh, Rakaposhi Range) and the boundary of ecumene. Abstracts for the International Symposium on "Karakorum-Hindukush-Himalaya: Dynamics of change, 29.9.–2.10.1995, Islamabad, p. 28.

Mejdahl, V., 1979. Thermoluminescence dating: beta attenuation in quartz grains. Archaeometry 21, 61–73.

Murray, A.S., Wintle, A.G., 2000. Luminescence dating of quartz using an improved single-aliquot regenerative-dose protocol. Radiation Measurements 32, 57–73.

Owen, L.A., 1994. Glacial and non-glacial diamictons in the Karakoram Mountains. In: Croots, D., Warren, W. (Eds.), The Deposition and Deformation of Tills. A.A, Balkema, Rotterdam, pp. 9–29.

Owen, L.A., Sharma, M.C., 1998. Rates and magnitudes of paraglacial fan formation in the Garhwal Himalaya. Geomorphology 26, 171–184.

Owen, L.A., Benn, D.I., Derbyshire, E., Evans, D.J.A., Mitchell, W., Sharma, M., Thompson, D., Lloyd, M., Richardson, S., 1995. The geomorphology and landscape evolution of the Lahul Himalaya, Northern India. Zeitschrift fur Geomorphologie 39, 145–174.

Owen, L.A., Finkel, R.C., Caffee, M.W., Gualtieri, L., 2002. Timing of multiple glaciations during the Late Quaternary in the Hunza Valley, Karakoram Mountains, Northern Pakistan: defined by cosmogenic radionuclide dating of moraines. Geological Society of America Bulletin 114 (5), 593–604.

Phillips, W.M., Sloan, V.F., Shroder Jr., J.F., Sha rma, P., Clarke, M.L., Rendell, H.M., 2000. Asynchronous glaciation at Nanga Parbat, northwestern Himalaya Mountains, Pakistan. Geology 28, 431–434.

Prescott, J.R., Hutton, J.T., 1994. Cosmic ray contributions to dose rates for luminescence and ESR dating: large depths and long-term time variations. Radiation Measurements 23, 497–500.

Richards, B.W.M., Owen, L.A., Rhodes, E.J., 2000a. Timing of Late Quaternary glaciations in the Himalayas of northern Pakistan. Journal of Quaternary Science 15, 283–297.

Richards, B.W.M, Benn, D., Owen, L.A., Rhodes, E.J., Spencer, J.Q., 2000b. Timing of Late Quaternary glaciations south of Mount

Everest in the Khumbu Himal, Nepal. Geological Society of America Bulletin 112 (10), 1621–1632.

Rose, J., Menzies, J., 1996. Glacial Stratigraphy. In: Menzies, J. (Ed.), Past Glacial Environments: Sediments, Forms and Techniques, vol. 2. Butterworth-Heinemann, Oxford, pp. 253–284.

Searle, M.P., 1991. The Geology and Tectonics of the Karakoram Mountains. Wiley, Chichester.

Shi Yafeng, Lui Xiaodong, Li Bingyuan, Yao Tandong, 1999. A very strong summer monsoon event during 30–40 ka BP in the Qinghai-Xizang (Tibet) Plateau and its relation to precessional cycle. Chinese Science Bulletin 44, 1851–1857.

Shi Yafeng, Yu Ge, Lui Xiaodong, Li Bingyuan, Yao Tandong, 2001. Reconstruction of the 30–40 ka BP enhanced Indian monsoon based on geological records from the Tibetan Plateau. Paleogreography, Palaeoclimatology, Palaeoecology 169, 69–83.

Tucker, M.E., 1982. The Field Description of Sedimentary Rocks. Geological Society of London Handbook Series, Vol. 1. Open University Press, Milton Keynes, 12pp.